Quantitative and time-resolved monitoring of organelle and protein delivery to the lysosome with a tandem fluorescent Halo-GFP reporter

M. Rudinskiy[a,b,c], T. J. Bergmann[a,b], and M. Molinari[a,b,d,*]
[a]Università della Svizzera italiana, CH-6900 Lugano, Switzerland; [b]Institute for Research in Biomedicine, CH-6500 Bellinzona, Switzerland; [c]Department of Biology, Swiss Federal Institute of Technology, CH-8093 Zurich, Switzerland; [d]School of Life Sciences, École Polytechnique Fédérale de Lausanne, CH-1015 Lausanne, Switzerland

ABSTRACT **Lysosomal degradative compartments hydrolyze macromolecules to generate basic building blocks that fuel metabolic pathways in our cells. They also remove misfolded proteins and control size, function, and number of cytoplasmic organelles via constitutive and regulated autophagy. These catabolic processes attract interest because their defective functioning is linked to human disease and their molecular components are promising pharmacologic targets. The capacity to quantitatively assess them is highly sought-after. Here we present a tandem-fluorescent reporter consisting of a HaloTag-GFP chimera appended at the C- or at the N-terminus of select polypeptides to monitor protein and organelle delivery to the lysosomal compartment. The Halo-GFP changes color on fluorescent pulse with cell-permeable HaloTag ligands and, again, on delivery to acidic, degradative lysosomal compartments, where the fluorescent ligand-associated HaloTag is relatively stable, whereas the GFP portion is not, as testified by loss of the green fluorescence and generation of a protease-resistant, fluorescent HaloTag fragment. The Halo-GFP tandem fluorescent reporter presented in our study allows quantitative and, crucially, time-resolved analyses of protein and organelle transport to the lysosomal compartment by high resolution confocal laser scanning microscopy, antibody-free electrophoretic techniques and flow cytometry.**

Monitoring Editor
Jennifer Lippincott-Schwartz
Howard Hughes Medical Institute

Received: Oct 29, 2021
Revised: Jan 19, 2022
Accepted: Jan 25, 2022

INTRODUCTION

Lysosomes are multifunctional organelles. Most notably, the luminal content in hydrolases and the low pH define their role as major catabolic compartment of nucleated cells, playing a crucial role in degradation and recycling of macromolecules (including proteins, lipids, and sugars), organelles, and pathogens (Shin and Zoncu, 2020). Defective lysosomal function due to impaired delivery of lysosomal enzymes or of the cargoes to be cleared from cells is associated with a large variety of human disorders (Hubner and Dikic, 2020; Szer and Peters, 2020; Yang and Klionsky, 2020; Parenti *et al.*, 2021). As such, monitoring transport events to lysosomes has attracted considerable interest as it allows to characterize trafficking pathways that converge to the catabolic organelles and to establish and evaluate pharmacologic approaches to modulate the function of key players.

Let us take delivery of misfolded proteins from the ER to acidic endolysosomes (ELs), or lysosomal turnover of ER portions as paradigms of trafficking and catabolic pathways, whose quantitative and kinetic assessment may offer important hints on cell physiology and pathology. Lysosome inactivation is a widely used, in some cases obligatory, experimental approach to gain this information because it preserves the cargoes delivered to acidic, degradative organelles that can directly be detected with various cell biology techniques including imaging and biochemical. Lysosomal

This article was published online ahead of print in MBoC in Press (http://www.molbiolcell.org/cgi/doi/10.1091/mbc.E21-10-0526) on February 2, 2022.

Author contributions: conceptualization: M.R., T.J.B., and M.M.; methodology: M.R., T.J.B., and M.M.; investigation: M.R., T.J.B., and M.M.; writing—original draft: M.R. and M.M.; writing—review and editing: M.R. and M.M.; supervision: M.M.

*Address correspondence to: M. Molinari (maurizio.molinari@irb.usi.ch).

Abbreviations used: BafA1, Bafilomycin A1; CLSM, confocal laser scanning microscopy; EL, endolysosome; ERLAD, ER-to-lysosome-associated degradation; FCS, fetal calf serum; GFP, green fluorescent protein; HBS, HEPES-buffered saline; HEK293, Human embryonic kidney 293; LSD, lysosomal storage disorder; MEF, mouse embryonic fibroblast; NEM, N-ethylmaleimide; PBS, phosphate-buffered saline; PNS, postnuclear supernatant; PS, permeabilization solution; PVDF, polyvinylidene difluoride; RFP, red fluorescent protein; TBS, Tris-buffered saline; TMR, tetramethylrhodamine.

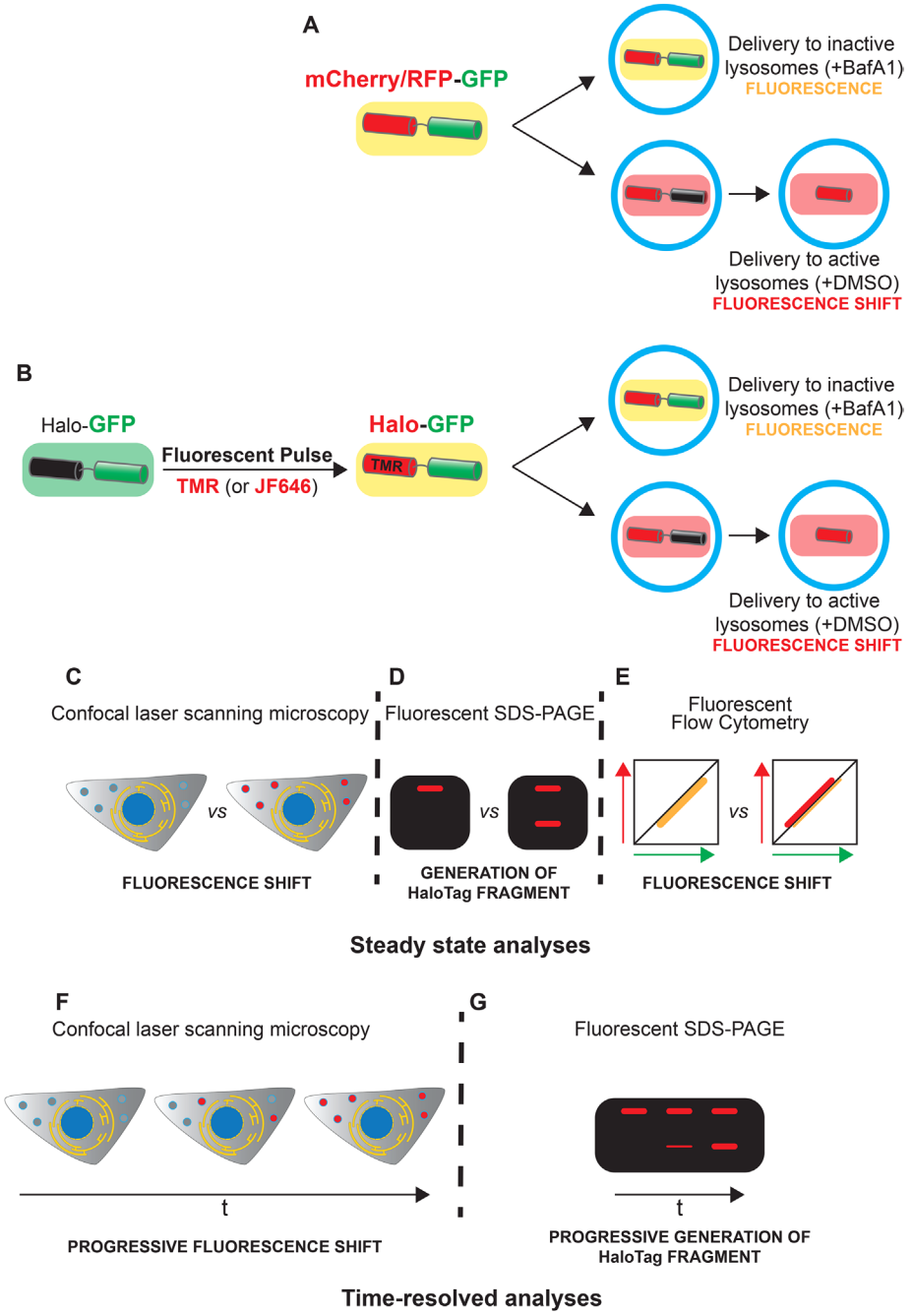

FIGURE 1: Tandem fluorescent reporters. (A) mCherry/RFP-GFP reporter. In inactive lysosomes (cells treated with BafA1) red and green fluorescence combine to yellow. In active lysosomes, GFP fluorescence is quenched, followed by the degradation of GFP moiety (red-only fluorescence). (B) Halo-GFP reporter. Same as A, but HaloTag is only fluorescent on cell incubation with fluorescent ligands (fluorescent pulse). Fluorescence, fluorescence shift, and generation of acid- and protease-resistant fluorescent HaloTag fragments can be observed in CLSM (C), in SDS–PAGE (D), flow cytometry assays (E). The combined use of fluorescent and nonfluorescent HaloTag ligands allows time-resolved analyses of protein and organelle delivery to lysosomes in CLSM (F) and in SDS–PAGE (G) as explained in the text and *Methods*.

inactivation is achieved on incubation of cultured cells with proton pump inhibitors such as Bafilomycin A1 (BafA1) or folimycin that neutralize the organelle pH (Hensens *et al.*, 1983; Bowman *et al.*, 1988; Woo *et al.*, 1992; Fregno *et al.*, 2018; Liang *et al.*, 2018; Loi *et al.*, 2019), or with protease inhibitors (e.g., with leupeptin) (Huisman *et al.*, 1974; Omari *et al.*, 2018; Kohno *et al.*, 2019). However, these approaches may elicit a number of unrelated cell responses (Klionsky *et al.*, 2008; Jacquin *et al.*, 2017). To circumvent this limitation, a series of tags that change their physicochemical properties in concomitance with the arrival in the acidic compartments have been developed and allow to perform studies in the absence of lysosomal inhibitors (Mizushima and Murphy, 2020). Among them, tandem fluorescent tags combine the red fluorescence of mCherry or of the red fluorescent protein (RFP) with the green fluorescence of the green fluorescent protein (GFP) (Figure 1A) (Kimura *et al.*, 2007; Pankiv *et al.*, 2007; Liang *et al.*, 2018; Chen *et al.*, 2019; Chino *et al.*, 2019; Liang *et al.*, 2020). When used in cells with inactive lysosomes (e.g., treated with BafA1), the combined red and green fluorescence accumulates within the Lamp1-positive organelles (Figure 1A, top part). Interestingly, however, mCherry and RFP are relatively stable in the lysosomal milieu, whereas GFP is acid and protease sensitive (Giepmans *et al.*, 2006; Ni *et al.*, 2011; Rodriguez *et al.*, 2017). Hence in cells with active lysosomes, one observes an overall persistence of the red fluorescence and a loss of the green fluorescence on cargo delivery in the lysosomal lumen (Figure 1A, bottom part). The limitation of these tandem fluorescent reporters is that they fail to inform on kinetics of the processes under investigation.

To overcome this, we replaced the mCherry/RFP parts of the tandem reporters with HaloTag (Figure 1B). HaloTag is a 33-kDa protein derived from the inactivated bacterial haloalkane dehalogenase. It is designed to covalently bind synthetic chloro- and bromoalkanes modified with a series of fluorescent (e.g., tetramethylrhodamine [TMR] or JF646, Figure 1B; hereafter TMR and JF646 refer to corresponding fluorescent dye–conjugated HaloTag ligands) or other functional ligands (Los *et al.*, 2008; England *et al.*, 2015). Like mCherry and RFP, HaloTag is relatively stable if compared with GFP and retains fluorogenic properties on arrival in the degradative, acidic organelles (Fregno *et al.*, 2018). Thus the substitution of the mCherry or RFP moieties of the conventional mCherry-GFP and RFP-GFP tandem reporters with HaloTag generates a tandem fluorescent Halo-GFP reporter that maintains the "color switch" testifying the arrival of the cargo to active ELs. Moreover, it confers the additional opportunity to pulse-label with cell permeable, fluorescent HaloTag ligands the newly synthesized protein of interest (Figure 1B) (Fregno *et al.*, 2018, 2021; Loi *et al.*, 2019). Denaturation and degradation of the GFP moiety on arrival to lysosomal compartments results in a fluorescence shift and

in the generation of an acid- and protease-resistant red fluorescent HaloTag fragment that can be revealed by confocal laser scanning microscopy (CLSM) (Figure 1C), gel electrophoresis (Figure 1D), and flow cytometry (Figure 1E) at steady state (Figure 1, C–E) as well as in time-resolved analyses (Figure 1, F and G).

The robustness of our approach has first been validated by quantitative and time-resolved analyses of delivery to ELs of ER portions as triggered by overexpression of Sec62, whose cytosolic C-terminus has been covalently modified by the addition of Halo-GFP. Sec62 is an ER-phagy receptor, whose overexpression mimics the fragmentation and delivery of excess ER portions to Rab7/Lamp1 ELs via piecemeal *micro*-ER-phagy, which is triggered during cell recovery from reversible ER stresses (hereafter recov-ER-phagy) (Fumagalli *et al.*, 2016; Loi *et al.*, 2019; Loi and Molinari, 2020). A second validation consisted in monitoring the clearance of ER portions containing proteasome-resistant misfolded polypeptides, as triggered on luminal expression of the disease-causing polymers of the Z-variant of alpha-1 antitrypsin (ATZ), a canonical client of ER-to-lysosome-associated degradation (ERLAD) (Fregno and Molinari, 2018, 2019; Fregno *et al.*, 2021). For this assay, Halo-GFP was appended at the N-terminus of ATZ.

RESULTS

Sec62-Halo-GFP reports on lysosomal delivery of ER portions during recov-ER-phagy: CLSM analyses

To validate the use of the Halo-GFP tag in reporting on magnitude and timing of organelle delivery to acidic degradative compartments, the Halo-GFP reporter was first appended at the cytosolic C-terminal domain of the ER-phagy receptor Sec62 (Figure 2A). The addition of C-terminal tags such as -HA, -Halo, or -GFP does not impair the function of Sec62 in driving delivery of ER portions to the endolysosomal compartments for clearance (Fumagalli *et al.*, 2016; Loi *et al.*, 2019). To confirm that this is also true for Halo-GFP, a plasmid for expression of the Sec62-Halo-GFP chimera was transiently transfected in mouse embryonic fibroblasts (MEF) seeded on glass coverslips. Ten hours posttransfection, the cell permeable HaloTag ligand TMR was added to the cell culture media, at a concentration of 100 nM, to generate a *yellow* (red (HaloTag-TMR) + green (GFP)) Sec62-Halo-GFP chimera. After 15 h in the presence of 50 nM BafA1 to inactivate lysosomal activity and preserve the Sec62-Halo-GFP chimeras delivered to ELs, cells were processed for CLSM as described in *Methods* and were stained with an antibody to the endolysosomal marker Lamp1 (Figure 2B). Consistent with expectations, the portions of ER displaying the ectopically expressed, *yellow*, Sec62-Halo-GFP chimera accumulate in the lumen of Lamp1-positive ELs (Figure 2B, inset).

Sec62 contains a phenylalanine-glutamic acid-methionine-isoleucine (-FEMI-) LC3-binding region (LIR in Figure 2A). Substitution of the -FEMI- tetrapeptide with a tetra-alanine (-AAAA-) sequence abolishes association of the cytosolic autophagic protein LC3 and inhibits Sec62-driven delivery of excess ER portions to Els for clearance (Fumagalli *et al.*, 2016; Loi *et al.*, 2019). Consistently, ectopic expression of Sec62LIR-Halo-GFP fails to induce delivery of ER portions, and of the associated yellow fluorescence, to Lamp1-positive Els (Figure 2C). Delivery of the Sec62-Halo-GFP-associated yellow fluorescence to the Lamp1-positive compartments is quantified by LysoQuant, an unbiased and automated deep learning image analysis tool for segmentation and classification of fluorescence images capturing cargo delivery to ELs (Figure 2, D and E) (Morone *et al.*, 2020). Thus the Sec62-Halo-GFP chimera is a reliable reporter of Sec62-regulated delivery of ER portions to degradative compartments, which rely on a functional LIR displayed by the ER-phagy receptor.

Next, we assessed the capacity of Sec62-Halo-GFP to report on recov-ER-phagy in cells with active ELs. In the absence of BafA1 (Figure 2, F–H), Lamp1-positive ELs are smaller (compare the Lamp1 channel in Figure 2, B and C vs. Figure 2, F and G) and the ER portions delivered to ELs are readily degraded (Fumagalli *et al.*, 2016; Loi *et al.*, 2019). The GFP fluorescence associated with the ER-phagy receptor Sec62 in the Halo-GFP chimera is rapidly quenched, whereas the more stable HaloTag portion preserves the red fluorescence conferred by the TMR ligand. All in all, in cells with active ELs, delivery of ER portions to the degradative compartment is testified by the accumulation of HaloTag-only (i.e., red fluorescent) puncta that colocalize with Lamp1-positive ELs (Figure 2, F and H). In cells transfected with Sec62LIR-Halo-GFP, which does not support ER delivery to ELs (Figure 2, C and D) (Fumagalli *et al.*, 2016; Loi *et al.*, 2019), the generation of HaloTag-only (red) puncta colocalizing with Lamp1-positive ELs is virtually absent (Figure 2, G and H). This confirms the robustness of the Sec62-Halo-GFP chimera in monitoring by CLSM the Sec62-regulated delivery of ER portions to the lysosomal compartment for clearance.

Sec62-Halo-GFP reports on lysosomal delivery of ER portions during recov-ER-phagy: biochemical analyses

To biochemically assess the delivery of ER portions displaying the Halo-GFP chimera to ELs, we relied again on the relative stability of the HaloTag portion of the Sec62-Halo-GFP chimera, which retains fluorogenic properties in the lumen of acidic and proteolytically active ELs. Human embryonic kidney 293 (HEK293) cells were transfected with a plasmid for expression of Sec62-Halo-GFP (Figure 2I, lanes 1 and 2) or of Sec62LIR-Halo-GFP (Figure 2I, lanes 3 and 4). Ten hours after transfection, the cell media were supplemented with 100 nM TMR to fluorescently label the HaloTag moiety of Halo-GFP. Cells were incubated without (lanes 1 and 3) or with 50 nM BafA1 to inactivate the lysosomes (lanes 2 and 4). After 15 h, cells were detergent-solubilized and proteins from postnuclear supernatants (PNS) were separated by SDS–PAGE. Fluorescently, (TMR)-labeled polypeptides were revealed by gel scanning with a 532-nm wavelength laser. The PNS of HEK293 cells expressing Sec62-Halo-GFP contains two fluorescently labeled polypeptides. The fluorescent polypeptide at 116 kDa corresponds to TMR-labeled full-length Sec62-Halo-GFP (Figure 2I, lane 1). The fluorescent polypeptide at 33 kDa corresponds to the pH- and protease-resistant HaloTag portion of the Halo-GFP chimera (Figure 2I, lane 1). This fragment is not generated when the hydrolysis of material delivered to ELs is inhibited on cell incubation with BafA1 (Figure 2, I, lane 2, and J). Generation of the 33-kDa proteolytic fragment corresponding to the TMR-labeled HaloTag portion of the chimera is substantially hampered (Figure 2, I, lane 3, and J) or abolished (lane 4) in cells expressing the LIR-variant of Sec62 (Sec62LIR-Halo-GFP), which fails to deliver ER portions to ELs. Thus the biochemical assays shown in Figure 2, I and J confirm that generation of a fluorescent HaloTag fragment correlates with the delivery of fluorescently labeled cargo-of-interest to ELs observed by CLSM (Figure 2, B–H).

Sec62-Halo-GFP reports on lysosomal delivery of ER portions during recov-ER-phagy: time-resolved CLSM analyses

To gain information on the kinetics of recov-ER-phagy as mimicked by the overexpression of the ER-phagy receptor Sec62 coupled with Halo-GFP, an information that, we remind, cannot be gained by using the conventional fluorescent tandem reporters such as mCherry-GFP or RFP-GFP, we employed the HaloTag pulse-chase protocol used in our laboratory (Fregno *et al.*, 2018, 2021; Loi *et al.*, 2019).

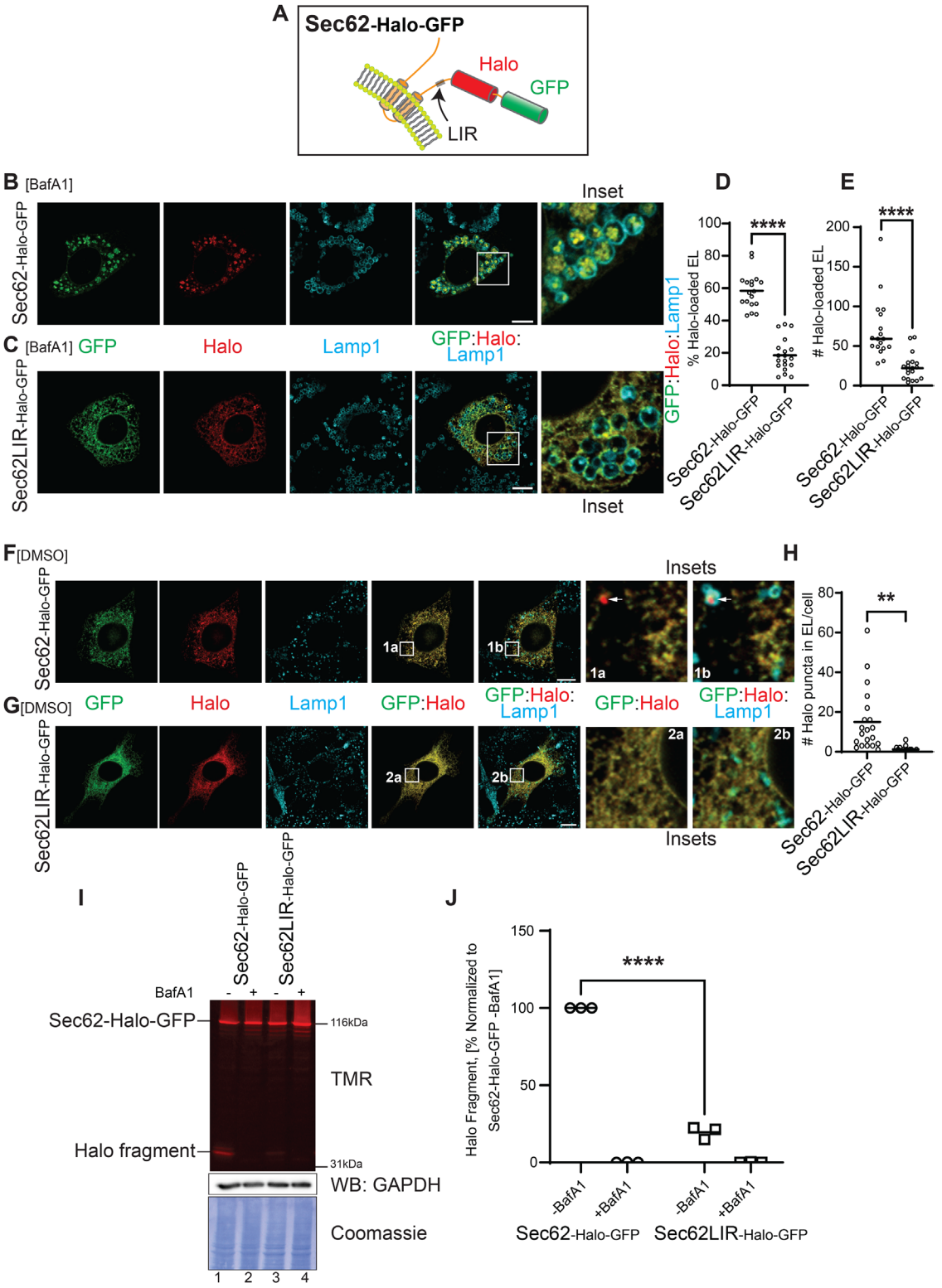

FIGURE 2: CLSM and biochemical analyses of Sec62-regulated ER-phagy. (A) Schematic representation of the membrane-bound Sec62-Halo-GFP chimera. The phenylalanine-glutamic acid-methionine-isoleucine (-FEMI-) LC3-interacting region (LIR) is indicated. (B) CLSM images of delivery of the Sec62-Halo-GFP chimera to Lamp1-positive endolysosomes (EL) in MEF cells treated with 50 nM BafA1 and 100 nM TMR for 15 h. (C) Same as B in cells expressing Sec62LIR-Halo-GFP. Scale bars: 10 µm; inset scale: 4× the magnification of merge images (D) LysoQuant quantification of the percentage of Halo-loaded Lamp1-positive EL in B and C (for Sec62-Halo-GFP [$n = 18$ cells], for Sec62LIR-Halo-GFP [$n = 19$ cells]). Unpaired two-tailed t test, ****$P < 0.0001$, mean bar is shown. (E) Same as D for the absolute number of Lamp1-positive Halo-loaded EL in B and C. Unpaired two-tailed t test, ****$P < 0.0001$, mean bar is shown. (F) Same as B in MEF cells incubated with 50 nM DMSO instead of BafA1. Arrows in the insets indicate HaloTag-only puncta in

Briefly, 17 h after transfection with the plasmid for expression of Sec62-Halo-GFP, MEF seeded on glass coverslips were treated with 15 µM 6-Chlorohexanol. This cell-permeable, nonfluorescent (*black*) ligand irreversibly occupies the HaloTag ligand binding pocket of the cellular pool of Sec62-Halo-GFP. After 30 min, the *black* ligand was replaced with 284 nM the cell-permeable, fluorescent JF646 ligand that covalently modifies the HaloTag of *newly* synthesized Sec62-Halo-GFP (fluorescent pulse). The fluorescent pulse was terminated after 1 h, when JF646 was washed out and replaced with 1.3 mM of the high-affinity *black* ligand 7-Bromo-1-heptanol (Merrill *et al.*, 2019) to block fluorescence incorporation. This initiates the chase time to monitor the fate of the pool of Sec62-Halo-GFP synthesized during the fluorescent pulse. At the end of each chase time (0, 2, 5, 7, or 10 h; Figure 3, A and B), cells were fixed and processed for CLSM as described in *Methods*. As in Figure 2, F and H, quantification of the time-dependent delivery of ER portions to the degradative compartment relies on the accumulation of HaloTag-only (red) puncta that colocalize with Lamp1-positive ELs. The quantitative analyses reveal the steady increase of JF646-labeled HaloTag within Lamp1-positive ELs (Figure 3B). These results mirror data previously obtained when the Sec62-regulated delivery of ER portions to the lysosomal compartment was monitored in cells exposed to BafA1 to inactivate lysosomal enzymes (Fumagalli *et al.*, 2016; Loi *et al.*, 2019) and support the robustness of the Halo-GFP chimera to monitor in a time-resolved manner the process of ER delivery to active ELs during Sec62-regulated ER-phagy.

Sec62-Halo-GFP reports on lysosomal delivery of ER portions during recov-ER-phagy: time-resolved biochemical analyses

Next, we combined the HaloTag pulse-chase protocol with the biochemical analyses that correlate the delivery of ER portions to the active ELs with the generation of fluorescent HaloTag proteolytic fragments (Figure 2, I and J). Seventeen hours after transfection of HEK293 cells with a plasmid for expression of the Sec62-Halo-GFP, the *black* ligand 6-Chloroxehanol was added to the cell culture media. The fluorescent pulse was performed by replacing 6-Chloroxehanol with 100 nM TMR for 1 h. Replacement of the TMR with the *black* ligand interrupts fluorescence incorporation and initiates the chase (0, 2, 5, 7, or 10 h; Figure 3, C and D). At the end of each chase time, cells were detergent-solubilized and fluorescent Sec62-Halo-GFP (fluorescent polypeptide at 116 kDa), as well as the fluorescent HaloTag fragment of 33 kDa generated on arrival of the Sec62-Halo-GFP chimera to active ELs, were separated in SDS–PAGE as described in Figure 2I (Figure 3C, lanes 1–5). Densitometric quantification of the fluorescent HaloTag fragment reveals its progressive generation during the chase (Figure 3D). A series of control experiments confirm our conclusions: first, in PNS from cells treated with 100 nM BafA1 to inactivate lysosomes, the fluorescent HaloTag fragment is not generated (Figure 3C, lane 6); second, Sec62-Halo-GFP and the HaloTag fragment are not fluorescent and therefore invisible in the gel on electrophoretic separation of PNS from cells not supplemented with the TMR ligand (lane 7); third, in cells transfected with superfolder GFP (sfGFP instead of Sec62-Halo-GFP) and incubated with TMR during the fluorescent pulse, no fluorescent polypeptide is visible in the gel (i.e., TMR specifically modifies the HaloTag-only) (lane 8); fourth, in cells expressing Sec62LIR-Halo-GFP the full-length reporter is fluorescently labeled, but the HaloTag fragment is not generated, consistent with the requirement of an active LIR domain in the Sec62 ER-phagy receptor to trigger recov-ER-phagy (lane 9). As a note, the time-resolved biochemical analyses (Figure 3, C and D) confirm, with higher sensitivity and multiple biological replicates, the results obtained by analyses of CLSM images (Figure 3, A and B). The apparent delay in red signal appearance within LAMP1-positive organelles (Figure 3B) should be ascribed to the lower sensitivity of this analytic method compared with time-resolved biochemical analyses (Figure 3, C and D).

Monitoring recov-ER-phagy as induced on Sec62 overexpression with quantitative single-cell flow cytometry assay

Finally, the use of the Sec62-Halo-GFP reporter to monitor ER delivery to ELs was validated by a flow cytometry assay (Figure 4). This assay, as with the previous ones, also relies on the low pH-induced quenching of the GFP fluorescence, which results in a red shift that we assessed in a single-cell high-throughput manner on a cell sorting analyzer. Briefly, HEK293 cells were transfected with a plasmid for expression of the Sec62-Halo-GFP (Figure 4, A and B) or of the Sec62LIR-Halo-GFP (Figure 4, C and D). Ten hours posttransfection, cells were incubated for 15 h with 100 nM TMR in the presence (top panels) or in the absence of 50 nM BafA1 (bottom panels). Cells were then gently detached from the dish, washed and subjected to fluorescent cell sorting as described in *Methods*. BafA1-treated cells (Figure 4, A and C) serve as a reference control. In these cells, lysosomes are inactive and the GFP fluorescence is not quenched. Under these conditions, red (TMR-linked HaloTag) and green (GFP) fluorescence levels are equivalent (Figure 4, A and C, yellow dots on the diagonal, below the gate). A small percentage of cells (5.44 and 5.76%, respectively, in this experiment) shows more intense red fluorescence and shows up in the gate. In the absence of BafA1, the fraction of fluorescent Sec62-Halo-GFP delivered to the ELs loses the GFP fluorescence, thus resulting in a significant red shift, which is shown by the presence of 30.5% of the cells in the gate (Figure 4, B and E for $N = 3$ biological replicates). As expected, the red shift is not observed in cells expressing the Sec62LIR-Halo-GFP chimera (Figure 4, D and E).

Halo-GFP-ATZ reports on lysosomal delivery of misfolded proteins: CLSM analyses

For quantitative and time-resolved analyses of a mechanistically different pathway of cargo delivery from the ER to ELs, we appended the Halo-GFP tag to the N-terminus of ATZ, a folding-defective, disease-causing variant of alpha1-antitrypsin (Figure 5A)

Lamp1-positive EL. (G) Same as F in cells expressing Sec62LIR-Halo-GFP. Scale bars: 10 µm; inset scale: 8× the magnification of merge images. (H) Quantification of HaloTag-only puncta colocalizing with EL in panels F and G (for Sec62-Halo-GFP [$n = 20$ cells], for Sec62LIR-Halo-GFP [$n = 16$ cells]). Unpaired Mann–Whitney two-tailed test, exact $^{**}P < 0.01$, median bar is shown. (I) Top panel: generation of the 33-kDa HaloTag fragment in HEK293 cells expressing Sec62-Halo-GFP (lanes 1, 2) or Sec62LIR-Halo-GFP (lanes 3, 4) and incubated with 100 nM TMR and 50 nM DMSO (lanes 1, 3) or BafA1 (lanes 2, 4) for 15 h. Middle panel: WB analysis showing GAPDH loading control shown as a reference. Bottom panel: PVDF membrane stained with Coomassie blue (loading control). (J) Quantification of the 33-kDa HaloTag fragment in I (fragment generated in cells expressing Sec62-Halo-GFP is set at 100%, $N = 3$ biological replicates). Two-way ANOVA with Sidak's multiple comparison test, $^{****}P < 0.0001$, mean bar is shown.

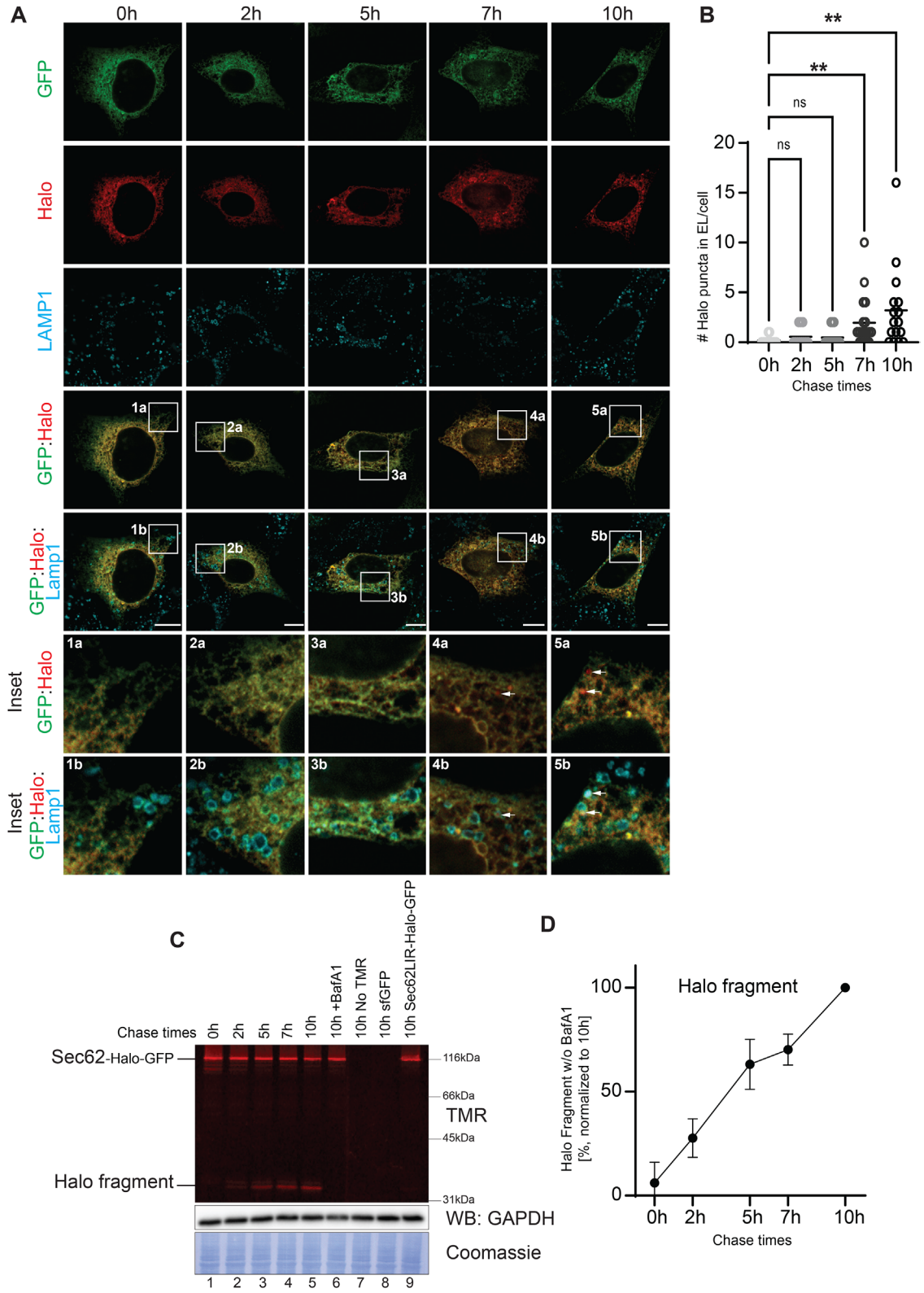

FIGURE 3: Time-resolved analyses of Sec62-Halo-GFP delivery to lysosomes. (A) MEF cells expressing Sec62-Halo-GFP and fluorescently pulse-labeled with the JF646 ligand to monitor the progressive formation of HaloTag-only puncta inside Lamp1-positive EL are fixed at 0, 2, 5, 7, and 10 h after the fluorescent pulse and processed for CLSM. Scale bar: 10 µm; inset scale: 4× the magnification of merge images. (B) Quantification of A ($n = 12$, 11, 13, 18, and 16 cells for the corresponding time points, $N = 1$). Kruskal–Wallis ANOVA test with Dunn's multiple comparison test. Adjusted $^{**}P < 0.01$; $^{*}P < 0.05$; ns, not significant; median bar is shown. (C) Generation of the fluorescent HaloTag fragment in HEK293 cells expressing Sec62-Halo-GFP at 0, 2, 5, 7, and 10 h after the fluorescent pulse (lanes 1–5). Controls are cells incubated with BafA1 (lane 6), not supplemented with the fluorescent HaloTag ligand TMR (lane 7), expressing sfGFP

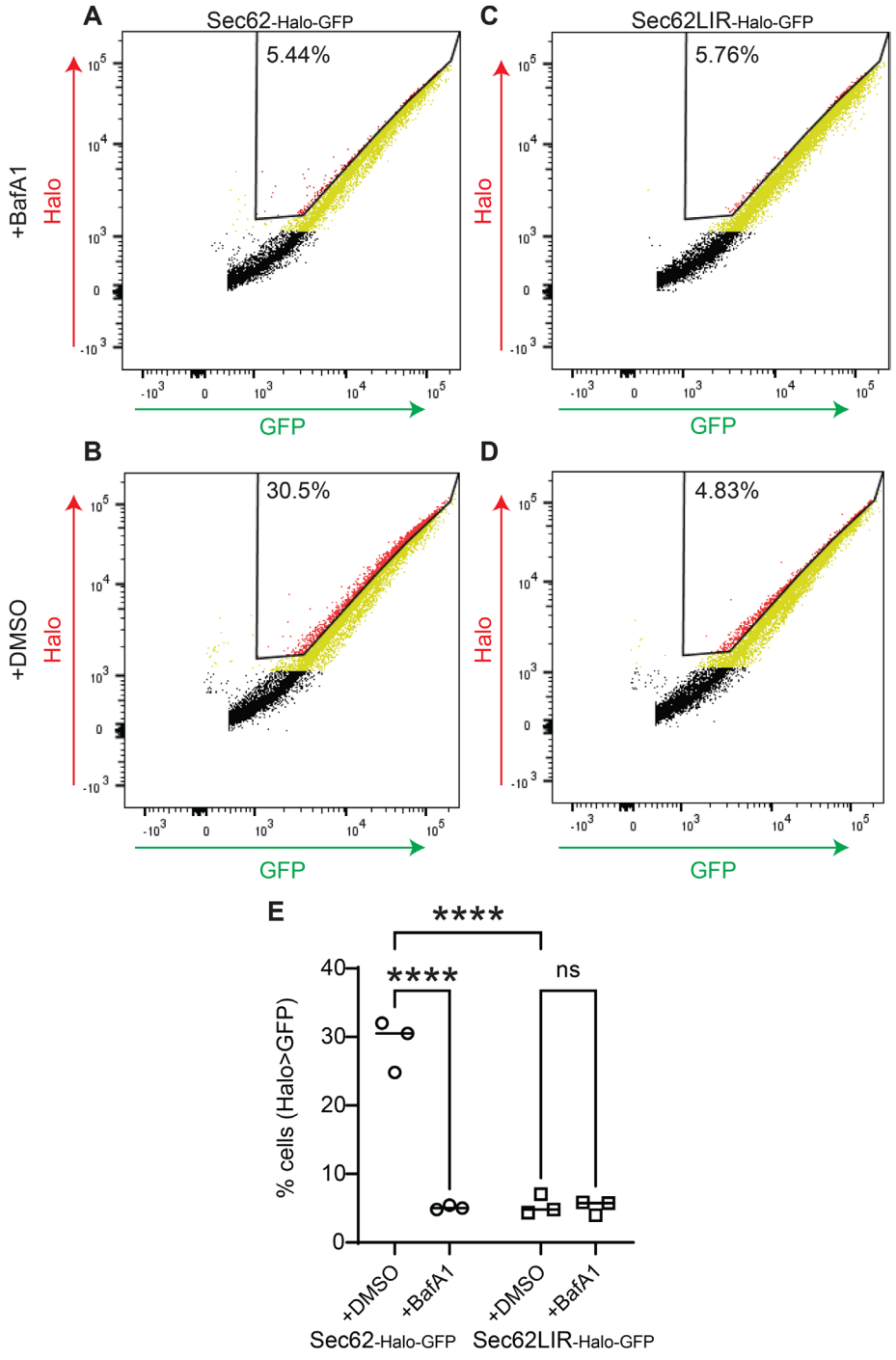

FIGURE 4: Quantitative flow cytometry assay of Sec62-Halo-GFP delivery to lysosomes. HEK293 cells expressing Sec62-Halo-GFP exposed to 50 nM BafA1 (A) or DMSO (B) and 100 nM TMR for 15 h were analyzed in flow cytometry. Halo and GFP fluorescences are plotted. Cells exhibiting quenching of green fluorescence are located inside the gate (red dots), and their percentage is displayed. Nontransfected cells were excluded from the analyses. (C) and (D) Same as A and B for HEK293 cells expressing Sec62LIR-Halo-GFP. (E) Statistical comparison of A–D, $N = 3$ biological replicates. Two-way ANOVA with Sidak's multiple comparison test, $N = 3$ biological replicates. ****$P < 0.0001$; ns, not significant, mean bar is shown.

(Strnad *et al.*, 2020). The fraction of ATZ that undergoes polymerization in the ER lumen is segregated in ER-derived vesicles that eventually fuse with ELs releasing ATZ polymers for ERLAD (Fregno & Molinari, 2018, 2019; Fregno *et al.*, 2021). As previously reported for the addition of N-terminal tags such as HA-, GFP-, or HaloTag-, also the Halo-GFP tag does not affect polymerogenicity of ATZ and delivery of the polymers to ELs for clearance (Supplemental Figure S1) (Miranda *et al.*, 2010; Fregno *et al.*, 2018, 2021). To follow delivery of Halo-GFP-ATZ polymers to ELs relying on the fluorescent signals generated by the Halo-GFP tag rather than on immunoreactivity, MEF transfected with a plasmid for expression of Halo-GFP-ATZ were incubated for 15 h with TMR for tandem fluorescent labeling of the chimera (red [HaloTag-TMR] + green [GFP]). Cells were grown in the presence of BafA1 to inhibit the clearance of the 2C1-positive Halo-GFP-ATZ polymers that are delivered to ELs (see Supplemental Figure S1, B and D) and were processed for CLSM analyses as described in *Methods*. The unbiased quantifications with LysoQuant reveal delivery of Halo-GFP-ATZ to ELs (Figure 5, B, D, and E). Much less fluorescence associated with the Halo-GFP-tagged Null-Hong-Kong (NHK) is detected within Lamp1-positive ELs (Figure 5, C–E) (Fregno *et al.*, 2021) (and unpublished from our lab). This was expected; in fact, NHK is a disease-causing, nonpolymerogenic variant of alpha1-antitrypsin, characterized by a frame shift mutation that results in premature chain termination at amino acid 333, misfolding, and degradation by the ubiquitin-proteasome system (Sifers *et al.*, 1988; Liu *et al.*, 1999).

Next, we evaluated the performance of the Halo-GFP-ATZ chimera to report on ERLAD in cells with active ELs. We are reminded that this test relies on the pH sensitivity of the GFP moiety of the chimera, which results in green fluorescence quenching. The analyses reveal the accumulation within Lamp1-positive ELs of HaloTag-only (red) puncta that colocalize with Lamp1-positive ELs (Figure 5, F and H). The negative control confirms that red-only fluorescent puncta are virtually absent in the Lamp1-positive compartment of cells expressing Halo-GFP-NHK (Figure 5, G and H).

(lane 8) or Sec62LIR-Halo-GFP (lane 9). Middle panel: WB of GAPDH as loading control shown as a reference. Bottom panel: PVDF membrane stained with Coomassie blue (loading control). (D) Quantification of C (lanes 1–5), $N = 3$ biological replicates, mean ± SD. The HaloTag peptide generated in cells expressing Sec62-Halo-GFP at 10 h chase is set at 100%.

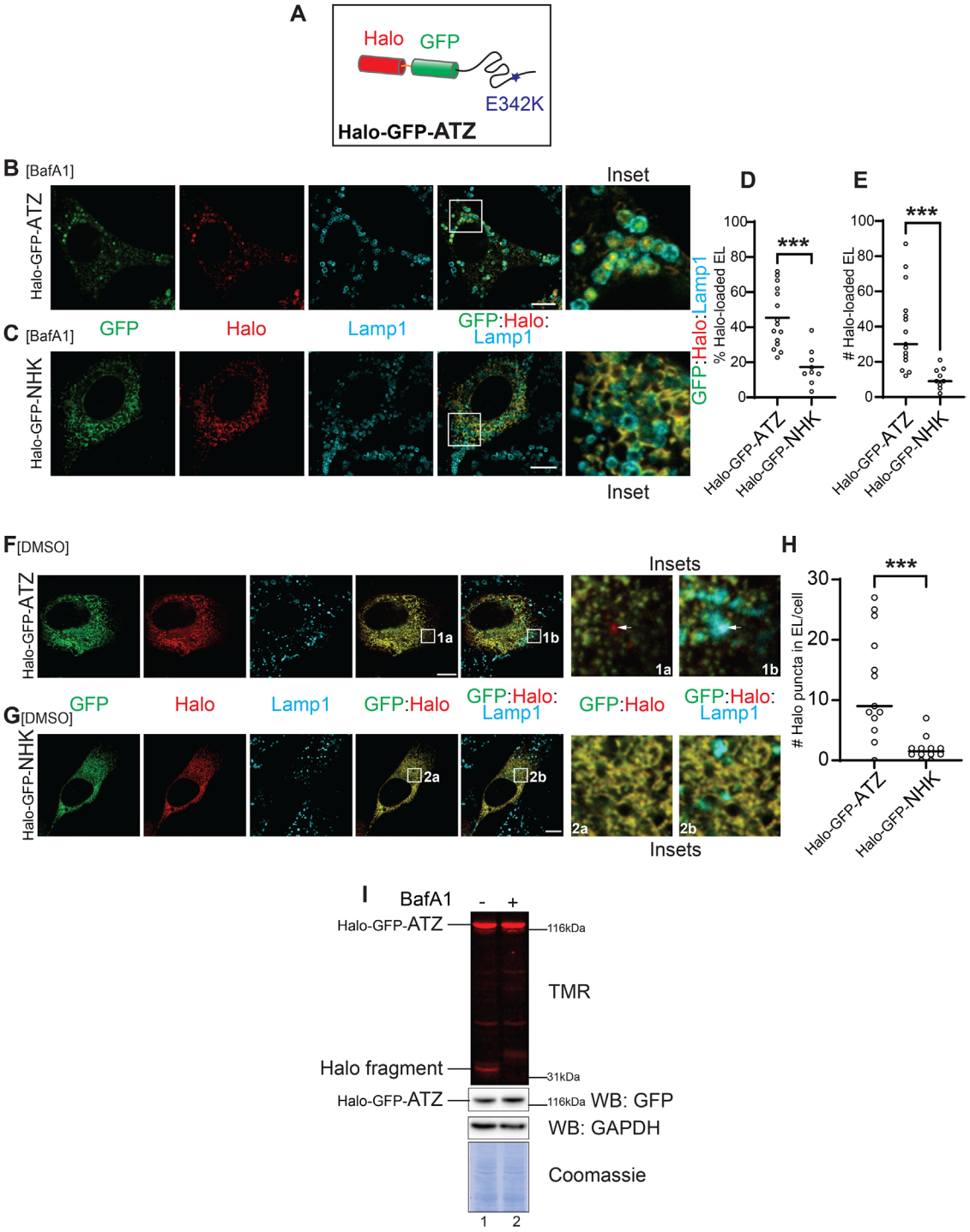

FIGURE 5: Delivery of Halo-GFP-ATZ polymers to lysosomes. (A) Schematic representation of Halo-GFP-ATZ. HaloTag (red) and GFP (green) moieties are appended to the N-terminus of ATZ, the disease-causing E342K mutation enhancing the polypeptide's polymerization propensity is shown. (B) Same as Figure 2B in MEF cells expressing Halo-GFP-ATZ exposed to 50 nM BafA1 and 100 nM TMR for 15 h. (C) Same as B in cells expressing Halo-GFP-NHK. Scale bars: 10 μm; inset scale: 4× the magnification of merge images. (D) LysoQuant quantification of the percentage of Halo-loaded Lamp1-positive EL in B ($n = 15$ cells) and C ($n = 9$ cells) in cells incubated with 50 nM BafA1. Unpaired two-tailed t test, $^{***}P < 0.001$, mean bar is shown. (E) Same as D for the absolute number of Lamp1-positive Halo-loaded Lamp1-positive EL in B and C. Unpaired two-tailed t test, $^{***}P < 0.001$, mean bar is shown. (F) Same as B in MEF cells not exposed to BafA1. Arrows indicate HaloTag-only puncta inside Lamp1-positive ELs. (G) Same as F in MEF cells expressing Halo-GFP-NHK. Scale bar: 10 μm; inset scale: 8× the magnification of merge images. (H) Quantification of F and G (number of HaloTag-only puncta inside Lamp1-positive EL, $n = 13$ cells expressing Halo-GFP-ATZ; $n = 12$ cells expressing Halo-GFP-NHK). Unpaired Mann–Whitney two-tailed test, exact $^{***}P < 0.001$, median bar is shown. (I) Top panel: generation of the 33-kDa HaloTag fragment on arrival of the Halo-GFP-ATZ chimera to acidic lysosomes in HEK293 cells not exposed

Halo-GFP-ATZ reports on lysosomal delivery of misfolded proteins: biochemical analyses

Lysosomal delivery of Halo-GFP-ATZ polymers in cells with active ELs was also assessed biochemically. HEK293 cells were transfected with the Halo-GFP-ATZ expression plasmid and fluorescently labeled 10 h posttransfection with 100 nM TMR in the presence or absence of BafA1. After 15 h, the cells were detergent-solubilized and the PNS was separated in SDS–PAGE. The fluorescent polypeptide bands corresponding to full-length Halo-GFP-ATZ and to the fluorescent protease- and acid-resistant HaloTag-fragment of 33 kDa are revealed by 532-nm laser scanning (Figure 5I, lane 1). The HaloTag fragment is virtually absent on inhibition of lysosomal hydrolases with BafA1, thus confirming that its generation depends on the delivery of Halo-GFP-tagged ATZ polymers to acidic ELs (Figure 5I, lane 2).

Halo-GFP-ATZ reports on lysosomal delivery of misfolded proteins: time-resolved CLSM analyses

We further investigated the kinetics of Halo-GFP-ATZ delivery to ELs by CLSM as shown above for the Sec62 chimera. MEF cells transfected with Halo-GFP-ATZ were incubated for 30 min with 15 µM of the *black* HaloTag ligand 6-Chlorohexanol before a 1-h fluorescent pulse of the newly synthesized pool of Halo-GFP-ATZ with 284 nM of the JF646 fluorescent HaloTag ligand. The fate of the JF646-labeled Halo-GFP-ATZ was monitored during a 0, 2, 5, 7, and 10 h chase initiated on substitution of the JF646 ligand with 1.3 mM of the *black* ligand 7-Bromo-1-heptanol. HaloTag-only (red) puncta appear within Lamp1-positive ELs 2 h after termination of the fluorescent pulse and their number peaks at 7 h (Figure 6, A, 0–10 h, and B). This testifies to the progressive delivery of the ERLAD client to ELs that results in quenching of the green fluorescence.

Halo-GFP-ATZ reports on lysosomal delivery of misfolded proteins: time-resolved biochemical analyses

Next, the kinetics of lysosomal delivery of Halo-GFP-ATZ polymers was assessed biochemically by monitoring the generation of the acidic- and protease-resistant fluorescent HaloTag fragment of 33-kDa. HEK293 cells transfected with Halo-GFP-ATZ were incubated with the *black* ligand 6-Chlorohexanol, pulse-labeled for 20 min with 100 nM TMR, and chased in the presence of 7-Bromo-1-heptanol. Cells were detergent-solubilized at 0, 2, 5, 7, and 10 h after the fluorescent pulse, and the PNS were subjected to SDS–PAGE followed by scanning of the gel with a 532-nm laser (Figure 6C). Delivery of Halo-GFP-ATZ polymers to acidic ELs results in the time-dependent formation of the HaloTag fragment that migrates a 33 kDa (Figure 6, C, HaloTag fragment panel, lanes 1–5, and D). The formation of the HaloTag fragment correlates with the formation of HaloTag-only puncta in CLSM (Figure 6, A and B). All in all, the results shown in Figures 5 and 6 confirm that the Halo-GFP tag allows quantitative time-resolved analyses of misfolded protein delivery to acidic degradative compartments.

Halo-GFP-ATZ reports on lysosomal delivery of misfolded proteins: quantitative single-cell flow cytometry assay

Finally, as described in Figure 4 for Sec62-Halo-GFP, we validated the delivery of Halo-GFP-tagged ATZ polymers to ELs in HEK293 cells with the cell sorting assay. We used Halo-GFP-tagged NHK as a control showing much reduced lysosomal delivery (Figure 5) (Fregno *et al.*, 2021) (and unpublished from our lab). The delivery of Halo-GFP-ATZ to active lysosomes is marked by quenching of GFP fluorescence resulting in a significant red shift in almost 40% of the transfected cells, which is abolished by neutralization of the lysosomal pH with BafA1 (Figure 7B vs. Figure 7, A and E for $N = 4$ biological replicates). As expected, the red shift indicative of lysosomal delivery is modest for Halo-GFP-NHK (Figure 7D vs. Figure 7, C and E).

DISCUSSION

The lysosome lumen is characterized by acidic pH and a high concentration of over 50 hydrolases including nucleases, lipases, glycosidases, sulfatases, phosphatases, and proteases (Lubke *et al.*, 2009). These enzymes are synthesized in the ER and are delivered to the degradative compartment via the secretory pathway. Their substrates include macromolecules, organelles and pathogens that originate from the extracellular or the intracellular milieu and are delivered to the degradative compartments via endocytic, secretory, and autophagic pathways (Shin and Zoncu, 2020). Quantitative and time-resolved analytic methods to monitor delivery to the lysosomal compartments of resident enzymes or of cargo to be cleared from cells are needed to mechanistically characterize trafficking pathways and to identify modulators that could open therapeutic avenues to treat lysosomal dysfunctions and lysosomal storage disorders (LSD) (Marques and Saftig, 2019). These may result from loss-of-function mutations in genes encoding a select lysosomal enzyme, or from defective delivery of macromolecules or organelles to be degraded. Here we have used the Halo-GFP chimera as a versatile fluorescent reporter for quantitative and time-resolved analyses of lysosomal delivery by fusing an acid- and protease-resistant HaloTag and an acid- and protease-sensitive GFP moiety to be appended to any protein of interest.

The concept at the foundation of our idea is the same that has been exploited by conventional tandem fluorescent reporters such as mCherry-GFP or RFP-GFP, where mCherry and RFP maintain their fluorescent properties within the acid and hydrolytic endolysosomal milieu, whereas the GFP fluorescence is quenched and the GFP portion of the chimera is proteolytically digested (reviewed in Giepmans *et al.*, 2006; Rodriguez *et al.*, 2017; Mizushima and Murphy, 2020; Molinari, 2021). The substitution of the mCherry/RFP part of the fluorescent tags with HaloTag offers advantages. First, the HaloTag is not fluorescent per se. Fluorescence is conferred by cell permeable ligands that can be added on demand to covalently and irreversibly occupy the HaloTag-binding site (Los *et al.*, 2008; England *et al.*, 2015). This allows to switch on the "tandem" fluorescence function of the Halo-GFP reporter on the addition of a series of cell permeable ligands with select fluorescent features and to switch it off by adding nonfluorescent ligands. This property valorizes our reporter when exploited in the context of fluorescent pulse labeling protocols, which allow time-resolved analyses in cells with functional lysosomes. Second, the plethora of HaloTag ligands that are commercially available expand the spectrum of use of the Halo-GFP tandem fluorescent reporter. In this work, the robustness of the Halo-GFP reporter has been assessed in CLSM, biochemistry, and flow cytometry. However, a use in (time-resolved) electron

to BafA1 (lane 1) or incubated with 50 nM BafA1 (lane 2). Middle panels: WB analyses showing recognition of Halo-GFP-ATZ with anti-GFP antibody and GAPDH loading control shown as a reference. Bottom panel: PVDF membrane stained with Coomassie blue (loading control), $N = 3$ biological replicates.

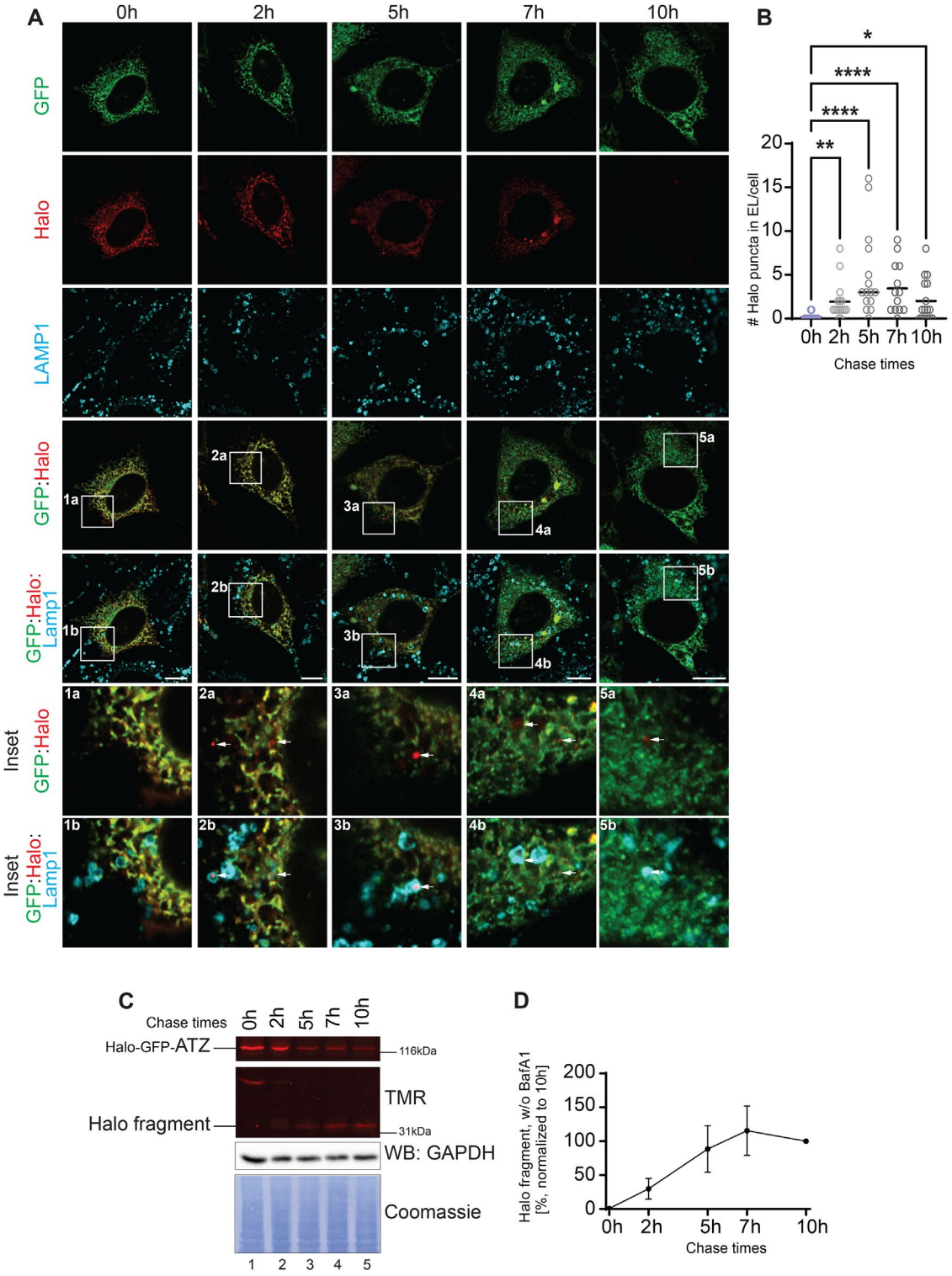

FIGURE 6: Time-resolved analyses of Halo-GFP-ATZ delivery to lysosomes. (A) Same as Figure 3A in MEF cells expressing Halo-GFP-ATZ to monitor the progressive appearance of Halo-positive puncta inside Lamp1-positive EL at 0, 2, 5, 7, and 10 h after the fluorescent pulse. (B) Quantification of A ($n = 15$, 16, 15, 13, and 16 cells for the corresponding time points, $N = 1$). Kruskal–Wallis ANOVA test with Dunn's multiple comparison. Adjusted $^{*}P < 0.05$; $^{**}P < 0.01$; $^{****}P < 0.0001$, median bar is shown. (C) Same as Figure 3C for HEK293 cells expressing Halo-GFP-ATZ to monitor the progressive generation of the 33-kDa HaloTag fragment at 0, 2, 5, 7, and 10 h after the fluorescent pulse. Middle panel: WB analysis showing GAPDH loading control shown as a reference. Bottom panel: PVDF membrane stained with Coomassie blue (loading control). (D) Quantification of (C). The HaloTag peptide generated in cells expressing Halo-GFP-ATZ after a 10 h chase is set at 100% ($N = 4$ biological replicates), mean ± SD.

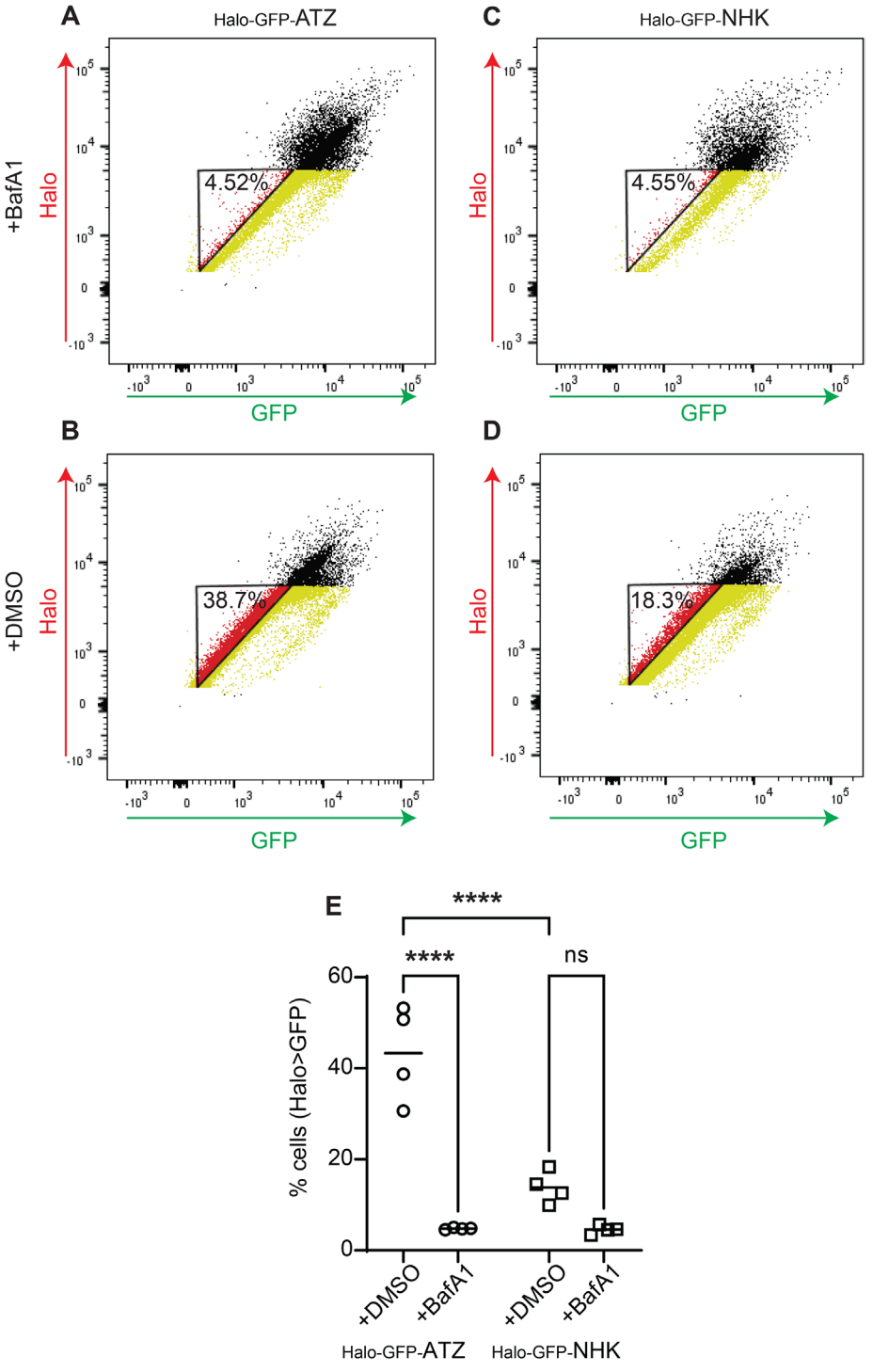

FIGURE 7: Quantitative flow cytometry assay of Halo-GFP-ATZ delivery to lysosomes. HEK293 cells expressing Halo-GFP-ATZ exposed to 100 nM TMR and 50 nM BafA1 (A) or DMSO (B) for 15 h were analyzed in flow cytometry. Halo and GFP fluorescences are plotted. Cells exhibiting quenching of green fluorescence are located inside the gate (red dots), and their percentage is displayed. Nontransfected cells (gray dots) and cells expressing high amounts of the ATZ chimera (black dots) were excluded from the quantitative analyses. (C) and (D) Same as A and B for HEK293 cells expressing Halo-GFP-NHK. (E) Statistical comparison of A–D, $N = 4$ biological replicates. Two-way ANOVA with Sidak's multiple comparison test, $N = 3$ biological replicates. ****$P < 0.0001$; ns, not significant, mean bar is shown.

microscopy is conceivable since the HaloTag ligand TMR photo-oxidizes diaminobenzidine to an osmiophilic polymer visible in transmission EM (Liss *et al.*, 2015).

In our work, we examine the fate of ER fragments decorated with the ER-phagy receptor Sec62 (Fumagalli *et al.*, 2016; Loi *et al.*, 2019; Loi & Molinari, 2020) and of the disease-causing protein ATZ, a defective gene product that enters polymers and is therefore not delivered to cytosolic proteasomes for ERAD. Instead, it is transported to ER-derived vesicles to the endolysosomal compartment for clearance via ERLAD (Fregno *et al.*, 2018, 2021; Fregno and Molinari, 2019). It is self-evident that the Halo-GFP tandem fluorescent reporter can be appended to resident lysosomal enzymes or to cargo proteins delivered alone, inside an organelle, or associated with a pathogen to be cleared from cells to quantitatively assess degradative pathways or trafficking from any intra- or extracellular site to the lysosomal compartment. As a select example of possible use of the Halo-GFP reporter that has not been examined in this work, it is worth mentioning that appending Halo-GFP to resident lysosomal enzymes and mutant forms thereof linked to LSD (Marques & Saftig, 2019) allows quantitative and time-resolved assessment of consequences on quality control and trafficking of the relevant mutation, the beneficial outcome of therapeutic treatments, and the high throughput/genomewide identification of perturbagens and alleviators of trafficking to lysosomal compartments, lysosomal function, and disease phenotypes.

METHODS

Request a protocol through *Bio-protocol*.

Expression plasmids and antibodies

ATZ and NHK were subcloned in pcDNA5 expression plasmid with the additions of a C-terminus HA tag and an N-terminus Halo-GFP tag. The HaloTag moiety is preceded by an ER-targeting Col2A1 signal polypeptide (-MAIRLGAPQTLVLLTLLVAAVLRCQG-) and an *Age*I restriction enzyme site (5′-accggtaac-3′). HaloTag and GFP are separated by a (-GSSGLRSAGPG-) linker containing *Hin*dIII restriction site followed by (-TSLYKKAGFPVAT-) attB1 Gateway cloning polypeptide (full linker DNA sequence: 5′-ggatcctccggactcagatccgctggcccaggaacaagtttgtacaaaaaagcaggctttccggtcgccacc-3′). The Halo-GFP tag is connected to the ATZ and NHK via a (-SGLRSGTEF-) sequence containing a *Kpn*I restriction enzyme site and flexible Gly-rich (-GGSGGSGG-) linker octapeptide (full linker DNA sequence: 5′-tccggactcagatccggtaccgaattcggtggatctggaggttctggtgga-3′). Sec62 and Sec62LIR constructs were subcloned in pcDNA3.1 expression plasmid with the addition of a C-terminus Halo-GFP tag, connected by a (-AAASG-) sequence

containing a *Not*I restriction enzyme site and a (-GGSGGSGG-) Gly-rich lysosome-sensitive octapeptide linker (full linker DNA sequence: 5′-gcggccgccagcggcggtggatctggaggttctggtgga-3′).

Commercial antibodies used in this study were against polymeric ATZ (2C1, HycultBiotech), GAPDH (Merck), HA (Sigma), Lamp1 (Hybridoma Bank, clone 1D4B, deposited to the DSHB by J. T. August), and GFP (Abcam). Alexa–conjugated secondary antibodies were purchased from Thermo Fisher Scientific, HRP–conjugated secondary antibodies were purchased from SouthernBiotech, and Protein A HRP–conjugated were purchased from Invitrogen.

Cell culture, transient transfection, and inhibitors

MEFs and HEK293 cells were grown in DMEM supplemented with 10% fetal calf serum (FCS) at 37°C and 5% CO_2. Transient transfections were performed using JetPrime transfection reagent (PolyPlus) as described in the manufacturer's protocol. BafA1 (Calbiochem), or DMSO (Sigma) were used at 50 nM for 15 h if not specified.

Cell lysis and Western blot

After the respective treatments, HEK293 cells were washed with ice-cold phosphate-buffered saline (PBS) containing 20 mM N-ethylmaleimide (NEM) then lysed with 2% CHAPS (in HEPES-buffered saline [HBS], pH 7.4) or RIPA buffer (1% Triton X-100, 0.1% SDS, 0.5% sodium deoxycholate in HBS, pH 7.4) supplemented with 20 mM NEM and protease inhibitors. PNS and lysis buffer-insoluble pellet were collected after centrifugation at 4°C 10,600 × *g* for 10 min. PNS was denatured for 5 min at 95°C with the addition of 100 mM dithiothreitol and subjected to SDS–PAGE. Following in-gel TMR imaging with Typhoon FLA 9500 (Software Version 1.0) with a 532-nm laser, proteins were transferred to polyvinylidene difluoride (PVDF) membranes using the Trans-Blot Turbo Transfer System (Bio-Rad). Membranes were blocked with 8% (wt/vol) nonfat dry milk (Bio-Rad) in Tris-buffered saline (TBS)-T and stained with primary antibodies diluted in TBS-T followed by HRP–conjugated secondary antibodies or HRP–conjugated Protein A diluted in TBS-T. Membranes were developed using Luminata Forte ECL detection system (Millipore) and signals were captured with FusionFX chemiluminescence imaging system (VILBER). TMR bands were quantified using the ImageQuant TL software (Molecular Dynamics, GE Healthcare).

Native gel electrophoresis

After CHAPS solubilization of HEK293 cells, PNS were incubated for 15 min at RT in native sample buffer (Bio-Rad) and subjected to 7.5% native nonreducing acrylamide gel in Tris/glycine buffer (Bio-Rad). Proteins were then transferred onto PVDF membrane in Tris/glycine buffer (Bio-Rad). Immunoblot analysis was performed as described above.

CLSM

MEFs were seeded on alcian blue-treated glass coverslips and transiently transfected with JetPrime reagent as described in the manufacturer's protocol. Ten hours after transfection, cells were treated with 50 nM DMSO or BafA1 for 15 h with 100 nM TMR HaloTag ligand (Promega). Cells were then washed in PBS and fixed at room temperature for 20 min in 3.7% formaldehyde diluted in PBS. Antigens were unmasked by incubating the coverslips for 15 min in permeabilization solution (PS, 0.05% saponin, 10% goat serum, 10 mM HEPES, 15 mM glycine). Cells were incubated with the primary antibodies diluted 1:100 in PS for 120 min, washed for three times in PS, and then incubated with Alexa Fluor–conjugated secondary antibodies diluted 1:300 in PS for 45 min. Cells were rinsed three times with PS and water and mounted with Vectashield (Vector Laboratories) supplemented with 40,6-diamidino-2-phenylindole (DAPI). Confocal images were acquired on a Leica TCS SP5 microscope with a Leica HCX PL APO lambda blue 63.0 × 1.40 OIL UV objective with pinhole 1 AU. Excitation was performed with 488-, 561-, and 633-nm lasers and fluorescence light was collected in 493–556, 566–628, and 640–702 nm ranges, respectively. Image analysis and quantification were performed with LysoQuant and FIJI (Morone *et al.*, 2020; Schindelin *et al.*, 2012). Image processing was also performed with Photoshop (Adobe).

Flow cytometry

HEK293 cells were seeded in a 24-well plate and transiently transfected with JetPrime reagent as described in the manufacturer's protocol. Ten hours after transfection, cells were treated with 50 nM DMSO or BafA1 for 15 h with 100 nM TMR HaloTag ligand (Promega). Cells were detached, washed three times in PBS, resuspended in MACS buffer (PBS with 2% FCS and 2 mM EDTA), and run on a Fortessa Cell Analyzer (BD Biosciences). Data were analyzed and graphical plots were created using FlowJo software (FlowJo LLC). During FlowJo analysis, cells expressing high amounts of Halo-GFP-ATZ and displaying GFP quenching in the presence of BafA1 were excluded from quantification.

Halo pulse-chase analysis

For CLSM analysis, MEFs cells were seeded on alcian blue coverslip and transiently transfected with Halo-GFP-ATZ or with Sec62-Halo-GFP as described above. Seventeen hours after transfection, cells were incubated for 30 min with 15 µM 6-Chlorohexanol (Sigma) in DMEM 10% FCS, a cell-permeable nonfluorescent HaloTag ligand that irreversibly occupies the HaloTag ligand-binding pocket. After two washes in DMEM 10% FCS, cells were incubated in the presence of 100 nM of BafA1 or DMSO for 60 min with 284 nM JF646 fluorescent HaloTag ligand (Promega) to exclusively label newly synthesized Halo-GFP-tagged proteins. After two washes in DMEM 10% FCS, the fluorescent ligand was replaced with 1.3 mM 7-Bromo-1-heptanol *black* HaloTag ligand to prevent incorporation of the fluorescent HaloTag ligand in the newly synthesized Halo-GFP-tagged proteins, with 100 nM BafA1 or DMSO. For biochemical analyses, HEK293 cells were transfected with Halo-GFP-tagged proteins and pulsed with HaloTag ligand TMR (Promega) for 20 min (for Halo-GFP-ATZ) or 60 min (Sec62-Halo-GFP). Cells were fixed or lysed after 0, 120, 300, 420, and 600 min of chase in the presence of 100 nM of BafA1 or DMSO and processed for confocal laser scanning imaging or for SDS–PAGE as reported above. For biochemical analyses, after SDS–PAGE gels were scanned with the Typhoon FLA 9500 (Software Version 1.0), bands were quantified using the ImageQuant software (Molecular Dynamics, GE Healthcare).

Statistical analysis

Statistical comparisons and graphical plots were performed using GraphPad Prism 9 (GraphPad Software Inc.). In this study, a one-way ANOVA Kruskal–Wallis test with Dunn's multiple comparison test (Figures 3B and 6B), a two-way ANOVA Sidak's multiple comparison test (Figures 4E and 7E), an unpaired Mann–Whitney two-tailed test (Figures 2H and 5H), and an unpaired two-tailed *t* test (Figures 2, D and E, and 5, D and E; Supplemental Figure S1D) were used to assess statistical significance. A P value < 0.05 (for unpaired two-tailed *t* test), an adjusted P value < 0.05 (for one-way ANOVA with Dunnett's multiple comparison test), a P value < 0.05 (for two-way ANOVA), and an exact P value < 0.05 (for Mann–Whitney test) were considered as statistically significant. All experimental replicates represent biological replicates; s.d., SD.

ACKNOWLEDGMENTS

We thank F. Reggiori, C. Settembre, and the members of Molinari's laboratory for discussions, and critical reading of the manuscript. M.M. is supported by the AlphaONE Foundation, the Foundation for Research on Neurodegenerative Diseases, the Swiss National Science Foundation (SNF), the Eurostars, Innosuisse, and the Comel and Gelu Foundations.

REFERENCES

Bowman EJ, Siebers A, Altendorf K (1988). Bafilomycins: a class of inhibitors of membrane ATPases from microorganisms, animal cells, and plant cells. Proc Natl Acad Sci USA 85, 7972–7976.

Chen QZ, Xiao Y, Chai PY, Zheng PL, Teng JL, Chen JG (2019). ATL3 is a tubular ER-phagy receptor for GABARAP-mediated selective autophagy. Curr Biol 29, 846–855.

Chino H, Hatta T, Natsume T, Mizushima N (2019). Intrinsically disordered protein TEX264 mediates ER-phagy. Mol Cell 74, 909–921.

England CG, Luo HM, Cai WB (2015). HaloTag technology: a versatile platform for biomedical applications. Bioconjugate Chemistry 26, 975–986.

Fregno I, Fasana E, Bergmann TJ, Raimondi A, Loi M, Solda T, Galli C, D'Antuono R, Morone D, Danieli A, *et al.* (2018). ER-to-lysosome-associated degradation of proteasome-resistant ATZ polymers occurs via receptor-mediated vesicular transport. EMBO J 37, e99259.

Fregno I, Fasana E, Solda T, Galli C, Molinari M (2021). N-glycan processing selects ERAD-resistant misfolded proteins for ER-to-lysosome-associated degradation. EMBO J 40, e107240.

Fregno I, Molinari M (2018). Endoplasmic reticulum turnover: ER-phagy and other flavors in selective and non-selective ER clearance. F1000Res 7, 454.

Fregno I, Molinari M (2019). Proteasomal and lysosomal clearance of faulty secretory proteins: ER-associated degradation (ERAD) and ER-to-lysosome-associated degradation (ERLAD) pathways. Crit Rev Biochem Mol Biol 54, 153–163.

Fumagalli F, Noack J, Bergmann TJ, Presmanes EC, Pisoni GB, Fasana E, Fregno I, Galli C, Loi M, Soldà T, *et al.* (2016). Translocon component Sec62 acts in endoplasmic reticulum turnover during stress recovery. Nat Cell Biol 18, 1173–1184.

Giepmans BN, Adams SR, Ellisman MH, Tsien RY (2006). The fluorescent toolbox for assessing protein location and function. Science 312, 217–224.

Hensens OD, Monaghan RL, Huang LY, Albersschonberg G (1983). Structure of the sodium and potassium-ion activated adenosine-triphosphatase inhibitor-L-681,110. J Am Chem Soc 105, 3672–3679.

Hubner CA, Dikic I (2020). ER-phagy and human diseases. Cell Death Differ 27, 833–842.

Huisman W, Lanting L, Doddema HJ, Bouma JMW, Gruber M (1974). Role of individual cathepsins in lysosomal protein digestion as tested by specific inhibitors. Biochim Biophys Acta 370, 297–307.

Jacquin E, Leclerc-Mercier S, Judon C, Blanchard E, Fraitag S, Florey O (2017). Pharmacological modulators of autophagy activate a parallel noncanonical pathway driving unconventional LC3 lipidation. Autophagy 13, 854–867.

Kimura S, Noda T, Yoshimori T (2007). Dissection of the autophagosome maturation process by a novel reporter protein, tandem fluorescent-tagged LC3. Autophagy 3, 452–460.

Klionsky DJ, Elazar Z, Seglen PO, Rubinsztein DC (2008). Does bafilomycin A(1) block the fusion of autophagosomes with lysosomes? Autophagy 4, 849–850.

Kohno S, Shiozaki Y, Keenan AL, Miyazaki-Anzai S, Miyazaki M (2019). An N-terminal-truncated isoform of FAM134B (FAM134B-2) regulates starvation-induced hepatic selective ER-phagy. Life Sci Alliance 2, e201900340.

Liang JR, Lingeman E, Ahmed S, Corn JE (2018). Atlastins remodel the endoplasmic reticulum for selective autophagy. J Cell Biol 217, 3354–3367.

Liang JR, Lingeman E, Luong T, Ahmed S, Muhar M, Nguyen T, Olzmann JA, Corn JE (2020). A genome-wide ER-phagy screen highlights key roles of mitochondrial metabolism and ER-resident UFMylation. Cell 180, 1160–1177.

Liss V, Barlag B, Nietschke M, Hensel M (2015). Self-labelling enzymes as universal tags for fluorescence microscopy, super-resolution microscopy and electron microscopy. Sci Rep 5, 17740.

Liu Y, Choudhury P, Cabral CM, Sifers RN (1999). Oligosaccharide modification in the early secretory pathway directs the selection of a misfolded glycoprotein for degradation by the proteasome. J Biol Chem 274, 5861–5867.

Loi M, Molinari M (2020). Mechanistic insights in recov-ER-phagy: micro-ER-phagy to recover from stress. Autophagy 16, 385–386.

Loi M, Raimondi A, Morone D, Molinari M (2019). ESCRT-III-driven piecemeal micro-ER-phagy remodels the ER during recovery from ER stress. Nat Commun 10, 5058.

Los GV, Encell LP, McDougall MG, Hartzell DD, Karassina N, Zimprich C, Wood MG, Learish R, Ohana RF, Urh M, *et al.* (2008). HaloTag: a novel protein labeling technology for cell imaging and protein analysis. ACS Chem Biol 3, 373–382.

Lubke T, Lobel P, Sleat DE (2009). Proteomics of the lysosome. Bba-Mol Cell Res 1793, 625–635.

Marques ARA, Saftig P (2019). Lysosomal storage disorders - challenges, concepts and avenues for therapy: beyond rare diseases. J Cell Sci 132, jcs221739.

Merrill RA, Song JN, Kephart RA, Klomp AJ, Noack CE, Strack S (2019). A robust and economical pulse-chase protocol to measure the turnover of HaloTag fusion proteins. J Biol Chem 294, 16164–16171.

Miranda E, Perez J, Ekeowa UI, Hadzic N, Kalsheker N, Gooptu B, Portmann B, Belorgey D, Hill M, Chambers S, *et al.* (2010). A novel monoclonal antibody to characterize pathogenic polymers in liver disease associated with alpha(1)-antitrypsin deficiency. Hepatology 52, 1078–1088.

Mizushima N, Murphy LO (2020). Autophagy assays for biological discovery and therapeutic development. Trends Biochem Sci 45, 1080–1093.

Molinari M (2021). ER-phagy responses in yeast, plants, and mammalian cells and their crosstalk with UPR and ERAD. Dev Cell 56, 949–966.

Morone D, Marazza A, Bergmann TJ, Molinari M (2020). Deep learning approach for quantification of organelles and misfolded polypeptide delivery within degradative compartments. Mol Biol Cell 31, 1512–1524.

Ni H-M, Bockus A, Wozniak AL, Jones K, Weinman S, Yin X-M, Ding W-X (2011). Dissecting the dynamic turnover of GFP-LC3 in the autolysosome. Autophagy 7, 188–204.

Omari S, Makareeva E, Roberts-Pilgrim A, Mirigian L, Jarnik M, Ott C, Lippincott-Schwartz J, Leikin S (2018). Noncanonical autophagy at ER exit sites regulates procollagen turnover. Proc Natl Acad Sci USA 115, E10099–E10108.

Pankiv S, Clausen TH, Lamark T, Brech A, Bruun JA, Outzen H, Overvatn A, Bjorkoy G, Johansen T (2007). p62/SQSTM1 binds directly to Atg8/LC3 to facilitate degradation of ubiquitinated protein aggregates by autophagy. J Biol Chem 282, 24131–24145.

Parenti G, Medina DL, Ballabio A (2021). The rapidly evolving view of lysosomal storage diseases. EMBO Mol Med 13, e12836.

Rodriguez EA, Campbell RE, Lin JY, Lin MZ, Miyawaki A, Palmer AE, Shu X, Zhang J, Tsien RY (2017). The growing and glowing toolbox of fluorescent and photoactive proteins. Trends Biochem Sci 42, 111–129.

Schindelin J, Arganda-Carreras I, Frise E, Kaynig V, Longair M, Pietzsch T, Preibisch S, Rueden C, Saalfeld S, Schmid B, *et al.* (2012). Fiji: an open-source platform for biological-image analysis. Nature Methods 9, 676–682.

Shin HR, Zoncu R (2020). The lysosome at the intersection of cellular growth and destruction. Developmental Cell 54, 226–238.

Sifers RN, Brashears-Macatee S, Kidd VJ, Muensch H, Woo SL (1988). A frameshift mutation results in a truncated alpha 1-antitrypsin that is retained within the rough endoplasmic reticulum. J Biol Chem 263, 7330–7335.

Strnad P, McElvaney NG, Lomas DA (2020). Alpha1-antitrypsin deficiency. The New England Journal of Medicine 382, 1443–1455.

Szer J, Peters H (2020). Treatable lysosomal storage diseases in the advent of disease-specific therapy. Intern Med J 50, 7–11.

Woo JT, Shinohara C, Sakai K, Hasumi K, Endo A (1992). Isolation, characterization and biological-activities of concanamycins as inhibitors of lysosomal acidification. J Antibiot 45, 1108–1116.

Yang Y, Klionsky DJ (2020). Autophagy and disease: unanswered questions. Cell Death Differ 27, 858–871.